LIMNOLOGY AND OCEANOGRAPHY
Letters

ASLO

Open Access

Limnology and Oceanography Letters 9, 2024, 442–451

doi: 10.1002/lol2.10397

LETTER

Weakening Indian Ocean carbon uptake in 2015: The role of amplified basin-wide warming and reduced Indonesian throughflow

Enhui Liao ,[1]* ***Wenfang Lu***,[2] ***Liang Xue*** ,[3] ***Yan Du***[4,5]

[1]School of Oceanography, Shanghai Jiao Tong University, Shanghai, China; [2]School of Marine Sciences, Sun Yat-Sen University, and Southern Marine Science and Engineering Guangdong Laboratory (Zhuhai), Zhuhai, China; [3]First Institute of Oceanography, Ministry of Natural Resources, Qingdao, China; [4]State Key Laboratory of Tropical Oceanography, SCSIO, CAS, Guangzhou, China; [5]University of Chinese Academy of Sciences, Beijing, China

Scientific Significance Statement

Ocean can greatly mitigate atmospheric CO_2 growth and associated climate warming by absorbing significant amounts of anthropogenic carbon. An accurate estimation of ocean carbon uptake is crucial for predicting future climate warming rates. However, the magnitudes and driving mechanisms of ocean carbon sink interannual variability remain poorly understood both at the global and basin scales. This study has identified an extraordinary air–sea CO_2 flux anomaly in the Indian Ocean during 2015 using multiple ocean CO_2 partial pressure (pCO_2) data and a state-of-the art ocean biogeochemical model. This extreme carbon flux anomaly, measuring up to 0.1 PgC/yr, has shifted the Indian Ocean from a carbon sink into a slight carbon source. An improved decomposition method is presented to examine the detailed driving processes of this ocean CO_2 anomaly. The results reveal that this extreme variability stems from distinctive processes: the extensive warming and unprecedented weakening of Indonesian Throughflow during the co-occurrence of Indian Ocean Dipole and extreme El Nino in 2015. The examination of this extreme CO_2 flux anomaly provides an important insight for a complete understanding of ocean carbon flux interannual variability in the Indian Ocean.

Abstract

In 2015, the Indian Ocean exhibits an exceptionally weakened CO_2 uptake, highlighting strong interannual variability of ocean carbon sink. By utilizing multiple ocean CO_2 partial pressure (pCO$_2$) data and a state-of-the-art ocean biogeochemical model, we show that the 2015 ocean CO_2 anomaly is characterized by a basin-wide amplification of ocean pCO$_2$, differing from ocean pCO$_2$ responses to other Indian Ocean Dipole events (e.g., 1997 and 2019). The distinct ocean pCO$_2$ anomaly is attributed to an amplified warming and an

*Correspondence: ehliao@sjtu.edu.cn

Associate editor: Alberto V. Borges

Author Contribution Statement: EL and YD conceived of the study. EL, WL and LX developed the conceptual framework. EL and WL compiled and analyzed all the data. EL wrote the first draft of the manuscript and all authors contributed to revisions.

Data Availability Statement: The MOM6 source code is publicly available at this site (https://github.com/NOAA-GFDL/MOM6-examples.git). The model data used in this study are publicly available on Zenodo (https://zenodo.org/record/8239409) under the https://doi.org/10.5281/zenodo.8239409. The Observational pCO$_2$-based products are available at https://www.nodc.noaa.gov/ocads/oceans/SPCO2_1982_present_ETH_SOM_FFN.html and https://doi.org/10.25921/m5wx-ja34. The OISST v2 SST data is available at https://www.ncei.noaa.gov/products/optimum-interpolation-sst.

Additional Supporting Information may be found in the online version of this article.

unprecedented weakening Indonesian Throughflow under the influence of co-occurrence of positive IOD and extreme El Niño in 2015. The amplified warming drives higher ocean pCO_2 in the western and central Indian Ocean, while the ITF transports anomalously high ocean pCO_2 water from the Pacific Ocean to the southeastern Indian Ocean. This newly identified ocean carbon response provides deeper insights into the Indian Ocean carbon interannual variability.

The ocean significantly mitigates atmospheric CO_2 growth and associated climate warming by absorbing ~ 39% of fossil carbon emissions since 1750 (Sabine et al. 2004; Friedlingstein et al. 2022; Gruber et al. 2023). Given the strong connection between atmospheric CO_2 levels and climate warming, accurately estimating ocean carbon uptake is crucial for predicting future climate warming rates. To enhance the precision of the ocean carbon uptake estimation, numerous studies have been conducted to understand the spatial and temporal variability of ocean carbon sink at global and basin scales (Le Quéré et al. 2000; Doney et al. 2009; Liao et al. 2020; McKinley et al. 2020; Chandra et al. 2022).

The air–sea CO_2 flux in the Indian Ocean (30° N–30° S), exhibits complex and intense interannual variability owing to compounded impact of Indian Ocean Dipole (IOD) and El Niño-Southern Oscillation (ENSO). However, our understanding of this variability remains limited, introducing notable uncertainties in accurately estimating the Indian Ocean carbon uptake. This CO_2 flux interannual variability has long been recognized in the Indian Ocean (Metzl et al. 1998). The Indian Ocean anomalously releases CO_2 to the atmosphere in the positive phase of IOD and takes up more CO_2 during the negative IOD on the basin scale (Sarma et al. 2023).

The impact of IOD on the air–sea CO_2 flux varies across different regions of Indian Ocean (Jabaud-Jan et al. 2004; Sarma 2006; Kartadikaria et al. 2015; Zhang et al. 2019; Valsala et al. 2020; Edwing et al. 2024). In the southeastern Indian Ocean, the ocean CO_2 partial pressure (pCO_2) anomaly is linked to anomalous upwelling, rainfall, and horizontal transport owing to wind anomaly driven by IOD (Rixen et al. 2006; Valsala et al. 2020). In the Arabian Sea, Sarma (2006) proposed that changes in biological processes might be responsible for the carbon flux anomaly during 1997 IOD. The southern Indian Ocean pCO_2 anomaly is primarily controlled by surface ocean warming/cooling associated with IOD (Jabaud-Jan et al. 2004; Zhang et al. 2019). ENSO is able to affect the Indian Ocean physical dynamics and might further influence carbon flux interannual variability when ENSO occurs alone or co-occurs with IOD (Guo et al. 2018).

The sensitivity of ocean carbon flux to IOD and ENSO is not yet comprehensively understood. After 1997–1998 El Niño, the 2015–2016 is the strongest El Niño year, exerting significant influences on the Pacific Ocean and adjacent oceans. The Indian Ocean (30° N–30° S) witnesses a unique IOD in 2015 with an extensive sea surface warming anomaly and an extreme weakening of Indonesian Throughflow (ITF) (Mayer et al. 2018; Zhang et al. 2018; Xiao et al. 2020; Jiang et al. 2022; Fritz et al. 2023; Huang et al. 2024; Yang et al. 2024). The ITF is a significant ocean current system that acts as a crucial pathway for global thermohaline circulation, transporting warm, fresh, and low-carbon water from the Pacific Ocean into the Indian Ocean. The interbasin exchange of heat, salinity, and carbon affects climate patterns (e.g., IOD and ENSO) and influences air–sea CO_2 flux and carbon balance between ocean basins. The unique event in 2015 is characterized as a monopole sea surface temperature (SST) anomaly, while the conventional IOD event, like 1997, exhibits a dipole SST anomaly. This distinct warming pattern plus an extreme weakening ITF might be responsible for the anomalous ocean carbon response in 2015. This work investigates how the distinct physical and biological changes drive air–sea CO_2 flux anomaly in the Indian Ocean underlying the influence of extreme El Niño and IOD in 2015.

Data and methods

Data and model

The observational pCO_2 data are too sparse to explore the interannual variability in the Indian Ocean (Supporting Information Fig. S1). To fully depict the variability, we analyze ocean pCO_2 and air–sea CO_2 flux from two reconstructed products: OS-ETHZ-GRaCER (Gregor and Gruber 2021) and SOM-FFN (Landschützer et al. 2014), both derived from Surface Ocean CO_2 Atlas (SOCAT) pCO_2 database (Bakker et al. 2016). Other datasets and data processing methods are described in Section S1 of the Supporting Information.

The study employs a global ocean/sea ice model coupled with a biogeochemical module from the Geophysical Fluid Dynamics Laboratory. The model includes modular ocean model version 6 (MOM6), sea ice simulator version 2, carbon ocean biogeochemistry, and lower trophics version 2 (COBALT v2), which is collectively referred to as MOM6-COBALT2 (Adcroft et al. 2019; Stock et al. 2020). The model performance is thoroughly assessed and it reproduces well-observed physical and biogeochemical features in the Indian Ocean, including both climatological mean state and interannual variability (Supporting Information Figs. S1–S8; Data S1). More detailed model evaluations and model configurations including spin-up, atmospheric forcing, and initial conditions, are referred to Section S2 of the Supporting Information and Liao et al. (2020).

Methods of examining changes in CO_2 flux and ocean pCO_2 anomalies

The variation in ocean pCO_2 is linked to changes in dissolved inorganic carbon (DIC), alkalinity (Alk), temperature (T), and salinity (S) through the following linear decomposition equation (Takahashi et al. 1993; Le Quéré et al. 2000).

$$\Delta pCO_{2w} \approx \underbrace{\frac{\partial pCO_{2w}}{\partial T}\Delta T}_{pCO_2-T} + \underbrace{\frac{\partial pCO_{2w}}{\partial DIC}\Delta DIC + \frac{\partial pCO_{2w}}{\partial Alk}\Delta Alk + \frac{\partial pCO_{2w}}{\partial S}\Delta S}_{pCO_2-NONT} \quad (1)$$

where pCO_{2w} denotes the ocean pCO_2. The four tracers are grouped into thermal (pCO_2-T) and nonthermal (pCO_2-NONT) components in Eq. (1). The driving processes of thermal and nonthermal components are shown in Eqs. (2) and (3), respectively.

$$\underbrace{(\partial_t pCO_{2w-T})}_{pCO_2-T\text{ tendency}} \approx \underbrace{\left(\frac{\partial pCO_{2w}}{\partial T} T_H\right)}_{TH_{circ}} + \underbrace{\left(\frac{\partial pCO_{2w}}{\partial T} T_V\right)}_{TV_{circ}} + \underbrace{\left(\frac{\partial pCO_{2w}}{\partial T} T_Q\right)}_{T_{flux}} \quad (2)$$

where subscript TH_{Circ} denotes the contribution from temperature horizontal transport (advection and diffusivity in the meridional and zonal directions), TV_{Circ} denotes the contribution from temperature vertical transport (vertical advection and diffusivity), and T_{flux} denotes the effect of surface heat flux.

$$\begin{aligned}\underbrace{(\partial_t pCO_{2w-NONT})}_{pCO_2-NONT\text{ tendency}} \approx & \underbrace{\left(\frac{\partial pCO_{2w}}{\partial DIC} DIC_H + \frac{\partial pCO_{2w}}{\partial Alk} Alk_H + \frac{\partial pCO_{2w}}{\partial S} S_H\right)}_{H_{Circ}} \\ & + \underbrace{\left(\frac{\partial pCO_{2w}}{\partial DIC} DIC_V + \frac{\partial pCO_{2w}}{\partial Alk} Alk_V + \frac{\partial pCO_{2w}}{\partial S} S_V\right)}_{V_{Circ}} \\ & + \underbrace{\left(\frac{\partial pCO_{2w}}{\partial DIC} DIC_{FW} + \frac{\partial pCO_{2w}}{\partial Alk} Alk_{FW} + \frac{\partial pCO_{2w}}{\partial S} S_{FW}\right)}_{FW} \\ & + \underbrace{\left(\frac{\partial pCO_{2w}}{\partial DIC} DIC_{Bio} + \frac{\partial pCO_{2w}}{\partial Alk} Alk_{Bio}\right)}_{Bio} + \underbrace{\left(\frac{\partial pCO_{2w}}{\partial DIC} DIC_{FCO_2}\right)}_{\text{Flux response}}\end{aligned} \quad (3)$$

As shown in Eq. (3), the time tendency of ocean pCO_2 nonthermal component (pCO_2-NONT tendency) is controlled by five terms: horizontal and vertical transport terms (H_{Circ} and V_{Circ}), the dilution/concentration effect (FW), the biological effect (Bio), and the influence of the air–sea CO_2 flux on pCO_{2w} (flux response). The detailed derivations of Eqs. (2) and (3) refer to Section S4.

Results

Extreme ocean carbon flux anomaly in 2015–2016

The Indian Ocean takes up atmospheric CO_2 (0.4–1 mol/m^2/yr) south of 15° S, while releasing carbon in the north, including the Arabian Sea and western Bay of Bengal (0.2–1 mol/m^2/yr) in the climatological mean status according to the two data products (Fig. 1). The balancing effect between southern and northern Indian Ocean makes the ocean basin a weak carbon sink (~0.1 PgC/yr, Supporting Information Fig. S9), consistent with synthesis result from Sarma et al. (2023). In 2015, anomalous CO_2 outgassing occurs across most of the Indian Ocean, including Arabian Sea (0.2–0.3 mol/m^2/yr), Bay of Bengal (0.1 mol/m^2/yr), southeastern Indian Ocean (0.3 molC/m^2/yr). The model captures this anomalous magnitude, but overestimates it in the Oman/Somali upwelling region. The significant CO_2 outgassing in the southeastern Indian Ocean coincides with a weakening of the ITF and South Equatorial Current, as shown in Fig. 1f.

As shown in Fig. 2a,b, the air–sea CO_2 flux anomaly integrated in the Indian Ocean varies from −0.1 to 0.1 PgC/yr between 1982 and 2020 according to the two data products (Landschützer et al. 2014; Gregor and Gruber 2021). The model demonstrates good agreement with the observed timing and magnitude of carbon flux interannual variability. The air–sea CO_2 flux anomaly shows relatively weak variations during the first half of 2015 (Fig. 2a), and then exhibits a significant increase from near zero to 0.1 PgC/yr during the second half of the year. After peaking in January 2016, the CO_2 flux gradually declines until July 2016 (Fig. 2a).

Most flux anomalies vary consistently with both IOD and Niño3.4 index (Fig. 2; Supporting Information Fig. S2). The CO_2 flux anomalies have a stronger response to the IOD ($y = 0.037x$, $r^2 = 0.43$) than the Niño3.4 ($y = 0.019x$, $r^2 = 0.44$, Supporting Information Fig. S2), suggesting that the IOD is the primary driving factor and the ENSO is an additional factor. However, the anomalous CO_2 flux in 2015 does not align well with the IOD strength (Fig. 2a, Supporting Information Fig. S2). The flux anomaly in 2015 is almost the maximum (0.1 PgC/yr) in the past 4 decades, while the IOD strength is only moderate (Fig. 2, Supporting Information Fig. S2). The extreme El Niño in 2015 might exert an additional influence on the extraordinary Indian Ocean CO_2 flux under the co-occurrence of IOD and El Niño.

The CO_2 flux anomaly in the Indian Ocean is primarily controlled by ocean pCO_2 variability (Fig. 2, Supporting Information Fig. S10, Section S3), which agrees with previous studies (Sarma 2006; Valsala and Maksyutov 2013; Valsala et al. 2021). The ocean pCO_2 anomaly exhibits consistent variation with CO_2 flux anomaly (Fig. 2c,d) in 2015. The ocean pCO_2 also peaks around 1998, 2010, and 2019, which aligns with the IOD and Niño3.4 index. This suggests that both the IOD and ENSO have a considerable influence on the ocean pCO_2 (Sarma 2006). Note that the Indian Ocean pCO_2 in 1991 did not show significant relation to the Pinatubo event, suggesting the complex role of the climate system in the regional ocean carbon cycle, which can lead to varied interpretations (McKinley et al. 2020; DeVries 2022).

The change in ocean pCO_2 is separated into two components: the pCO_2-T and pCO_2-NONT, according to Eq. (1).

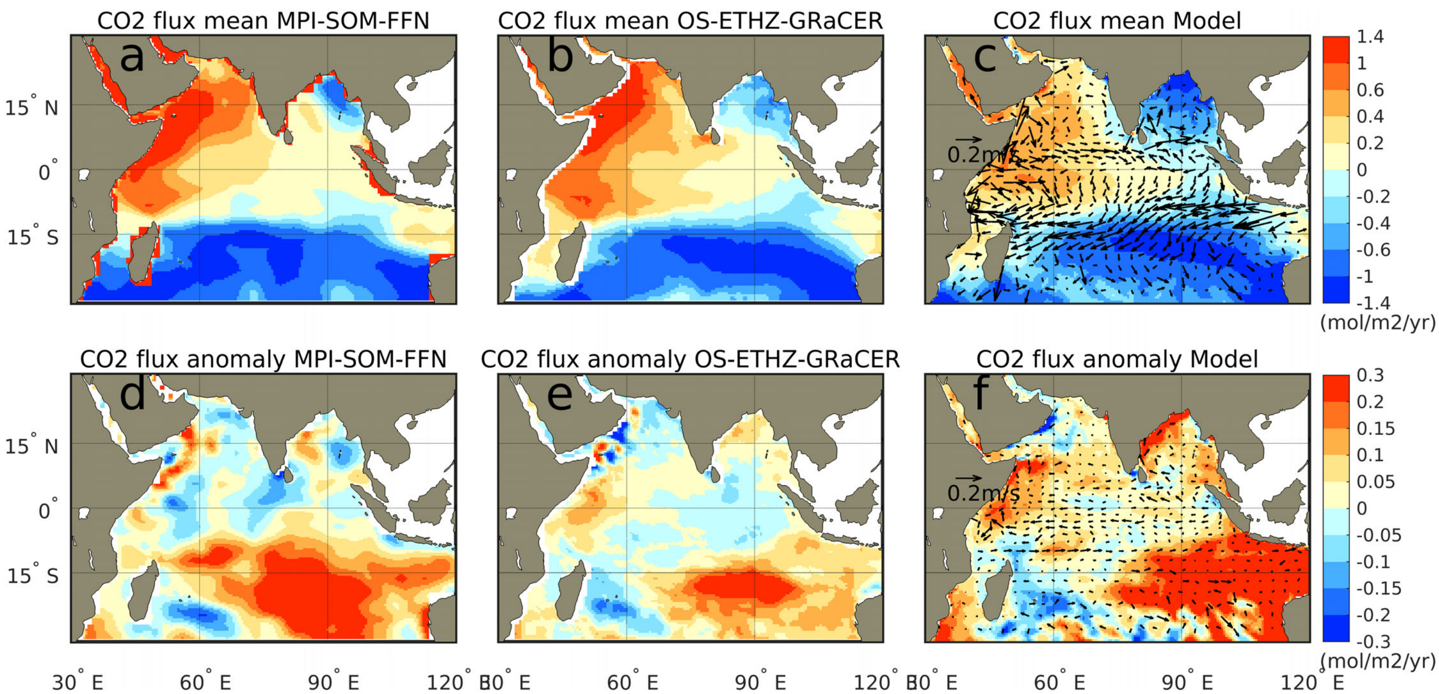

Fig. 1. Air–sea CO_2 flux map of climatological annual mean (**a–c**) and 2015 interannual anomaly (**d–f**) between data products and MOM6-COBALT. A positive flux denotes an outgassing from the ocean to atmosphere. In panel (a), AS, BoB, SEIO denote Arabian Sea, Bay of Bengal, and southeastern Indian Ocean respectively. Sumatra, Java, SS, LS, and TS represent Sumatra island, Java island, Lombok Strait, Sunda Strait, and Timor Sea respectively. Arrows in panel (c and d) depict the ocean circulation of climatological annual mean and interannual anomaly for 2015, derived from MOM6-COBALT. Data products are from MPI SOM-FFN and OS-ETHZ-GRaCER. The interannual anomaly is averaged between August 2015 and July 2016.

During 2015–2016, the pCO$_2$-T explains 91.5% of the variance in ocean pCO$_2$ (Fig. 2d). At the peak point of ocean pCO$_2$ anomaly around January 2016, the ocean pCO$_2$-T reaches as high as 9 μatm, while the pCO$_2$-NONT compensates for the SST effect with a magnitude of -3 μatm. As a result, the weakened ocean carbon flux is largely attributed to the high SST anomaly in 2015–2016 in the Indian Ocean. The detailed roles of pCO$_2$-T and pCO$_2$-NONT in different regions will be examined in the following section.

Two regions controlled by different mechanisms

From August 2015 to January 2016, an increasing ocean pCO$_2$ anomaly (positive, 5–15 μatm) is found in most of the Indian Ocean (Fig. 3a), except for the central Indian Ocean (70° E–80° E) and central Bay of Bengal. As a comparison, the high ocean pCO$_2$ anomaly (10–20 μatm) only appears in the eastern Indian Ocean, while the western Indian Ocean exhibits a negative ocean pCO$_2$ anomaly during a composited IOD between 1997 and 2019 (Fig. 3d). As the SST anomaly and other physical forcing (wind, upwelling, precipitation) show a conventional response to the IOD in 1997 and 2019 (Aparna et al. 2012; Guo et al. 2015), we consider these two events as conventional IOD and the ocean pCO$_2$ anomaly in 1997 and 2019 as representative of a typical pattern owing to a positive IOD.

Note that a well-known conventional ocean pCO$_2$ pattern driven by IOD is not extensively defined in the literature owing to data scarcity. Valsala et al. (2020) showed a model-based ocean pCO$_2$ response similar to the findings in the composited IOD between 1997 and 2019, which confirms the definition of typical ocean pCO$_2$ pattern in this study. Additionally, we examined the ocean pCO$_2$ responses to IOD and El Niño co-occurrence (pure positive IOD, pure El Niño, and combined positive IOD and El Niño, Supporting Information Fig. S11). The examination indicates two groups of ocean pCO$_2$ pattern similar to Fig. 3a,d (see details in Supporting Information Section S5). This further supports a definition of conventional ocean pCO$_2$ pattern with a positive and negative ocean pCO$_2$ anomaly in the eastern and western Indian Ocean, respectively (Fig. 3d).

The comparison highlights that the distinct feature of 2015 is the widespread elevated ocean pCO$_2$ on a basin scale. In the southeastern Indian Ocean, the positive ocean pCO$_2$ anomaly in 2015 extends along Java Island (90–120° E, 5–20° S) within a range of 6–18 μatm. In contrast, during a conventional IOD, the elevated ocean pCO$_2$ is located further north along Sumatra Island (90–110° E, 5° N–8° S). In the Bay of Bengal, the ocean pCO$_2$ has a similar response to both the 2015 IOD and conventional IOD. The high ocean pCO$_2$ anomaly in the western Bay of Bengal during 2015 is consistent with the

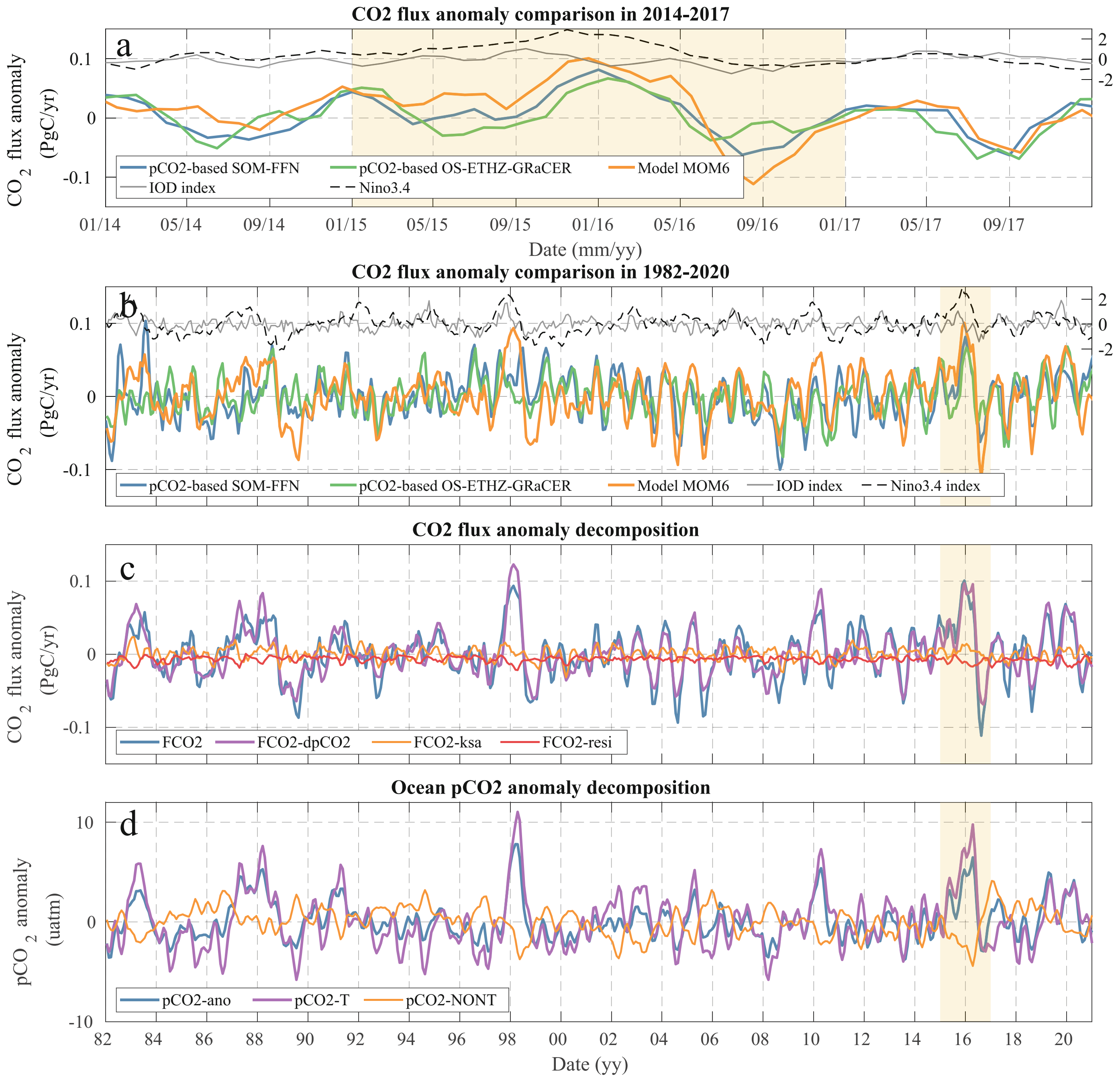

Fig. 2. Time series of air–sea CO_2 flux interannual anomaly in 2014–2017 (**a**) and 1982–2020 (**b**), decompositions of simulated air–sea CO_2 flux anomaly (**c**), and decomposition of simulated ocean pCO_2 anomaly (**d**). A positive flux denotes an anomalous outgassing from the ocean to atmosphere. The air–sea CO_2 flux and ocean pCO_2 anomalies are all integrated or averaged in the Indian Ocean. The decompositions of CO_2 flux and ocean pCO_2 anomalies are based on Eq. (S5) and Eq. (1), respectively. The yellow shading color highlights the specific period of interest (2015–2016) when the focused IOD occurs.

findings from earlier studies (Sarma et al. 2015; Shanthi et al. 2022).

In the northern Arabian Sea, the ocean pCO_2 increases dramatically (5–15 μatm) in the 2015 IOD, compared with a more modest increase (2–8 μatm) in the conventional IOD like 1997 and 2019 (Sarma 2006). In the southern Arabian Sea and western equatorial Indian Ocean, the ocean pCO_2 anomaly is positive during 2015, which is significantly different from the pattern in the conventional IOD. The ocean pCO_2 response to the conventional IOD in the northern Arabian Sea shows a

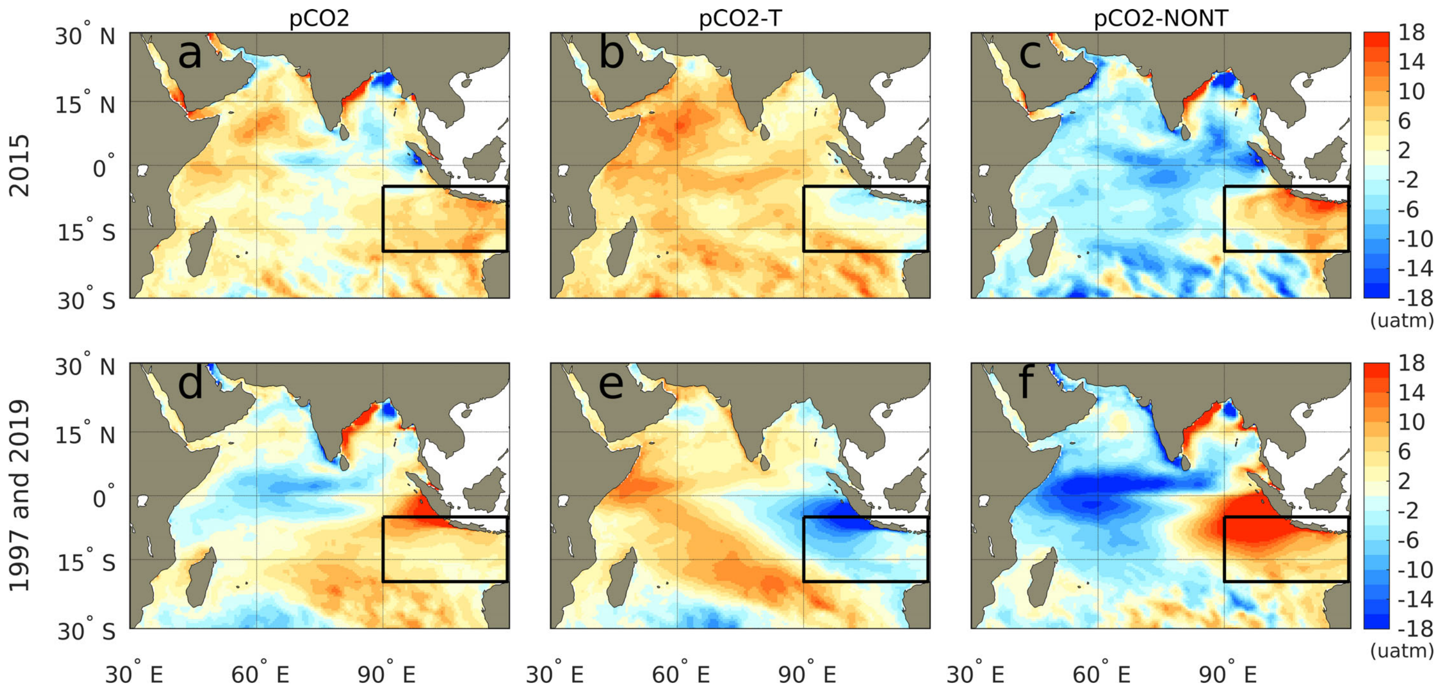

Fig. 3. Ocean $p\mathrm{CO_2}$ anomaly and its two components: $p\mathrm{CO_2}$-T and $p\mathrm{CO_2}$-NONT during 2015 (**a–c**) and for composite mean in 1997 and 2019 (**d**,**e**). The values are averaged from August to the following January for each IOD event. The ocean $p\mathrm{CO_2}$ anomaly is decomposed into two components: $p\mathrm{CO_2}$-T and $p\mathrm{CO_2}$-NONT according to Eq. (1). The black box indicates the $p\mathrm{CO_2}$-NONT region, while the left region is defined as $p\mathrm{CO_2}$-T region.

consistency with Sarma (2006), but a marginal discrepancy in the southern Arabian Sea. The marginal discrepancy might be attributed to the factor that Sarma (2006) focused solely on the 1997 event, whereas this study presents a composite analysis of events between 1997 and 2019.

The majority of positive ocean $p\mathrm{CO_2}$ is contributed by the $p\mathrm{CO_2}$-T component in most parts of the Indian Ocean (Fig. 3b) and the $p\mathrm{CO_2}$-NONT only contributes to the positive ocean $p\mathrm{CO_2}$ in the southeastern Indian Ocean (Fig. 3c). To better illustrate the dynamics, the Indian Ocean is divided into two subregions: $p\mathrm{CO_2}$-T region (the region outside of the black box in Fig. 3) and $p\mathrm{CO_2}$-NONT region (within the black box in Fig. 3), depending on their contribution to positive ocean $p\mathrm{CO_2}$ anomaly. The $p\mathrm{CO_2}$-T region accounts for $\sim$ 80% of the $\mathrm{CO_2}$ flux anomaly, while the $p\mathrm{CO_2}$-NONT region contributes to the remaining 20% of the $\mathrm{CO_2}$ flux anomaly.

The west and central Indian Ocean $p\mathrm{CO_2}$ anomaly driven by heat flux

In the $p\mathrm{CO_2}$-T region, the ocean $p\mathrm{CO_2}$ increases slowly in January–July 2015 and experiences rapid growth between August 2015 and January 2016 (Fig. 4a). As shown in the time series of budget terms, the fast-growing ocean $p\mathrm{CO_2}$ is largely forced by surface heat flux (Heat flux) between August 2015 and January 2016 (Fig. 4b,d). The heat flux term contributes to a positive $p\mathrm{CO_2}$-T tendency of 1.0 μatm/month. The horizontal ($\mathrm{H_{circ}}$) and vertical ($\mathrm{V_{circ}}$) transport terms offset the heat flux term by -0.1 and -0.6 μatm/month, respectively. The net effect of these three processes increases the $p\mathrm{CO_2}$ tendency by 0.3 μatm/month in the $p\mathrm{CO_2}$-T region (western and central Indian Ocean).

The ocean $p\mathrm{CO_2}$-T budget analysis aligns with previous studies related to the SST budget analysis during the positive IOD (Du et al. 2013). The Indian Ocean surface warming is largely contributed by heat flux in most of the Indian Ocean (e.g., Arabian Sea) and vertical transport in the western equatorial Indian Ocean (Supporting Information Figs. S12, S13). The heat flux warms the surface ocean through the wind-evaporation-SST (WES) feedback. Under the combined influence of IOD and El Niño, a cyclonic wind anomaly occurs in the western and central Indian Ocean in 2015, which weakens the South Asian summer monsoon and surface evaporation (Zhang et al. 2018; Jiang et al. 2022).

The southeastern Indian Ocean $p\mathrm{CO_2}$ anomaly driven by horizontal transport and rainfall

In the $p\mathrm{CO_2}$-NONT region, the temporal variability of ocean $p\mathrm{CO_2}$ exhibits a resemblance to the $p\mathrm{CO_2}$-T region, characterized by a slight rate of change during the first half of 2015 and a notably accelerated rate during the second half of the year (Fig. 4a). The fast-growing ocean $p\mathrm{CO_2}$-NONT is primarily attributed to the horizontal transport term ($\mathrm{H_{circ}}$, Fig. 4e). Although the vertical transport term ($\mathrm{V_{circ}}$) manages to counterbalance the horizontal transport term ($\mathrm{H_{circ}}$) in the summer of 2015 (August and September), it quickly diminishes afterward. Consequently, the horizontal transport term

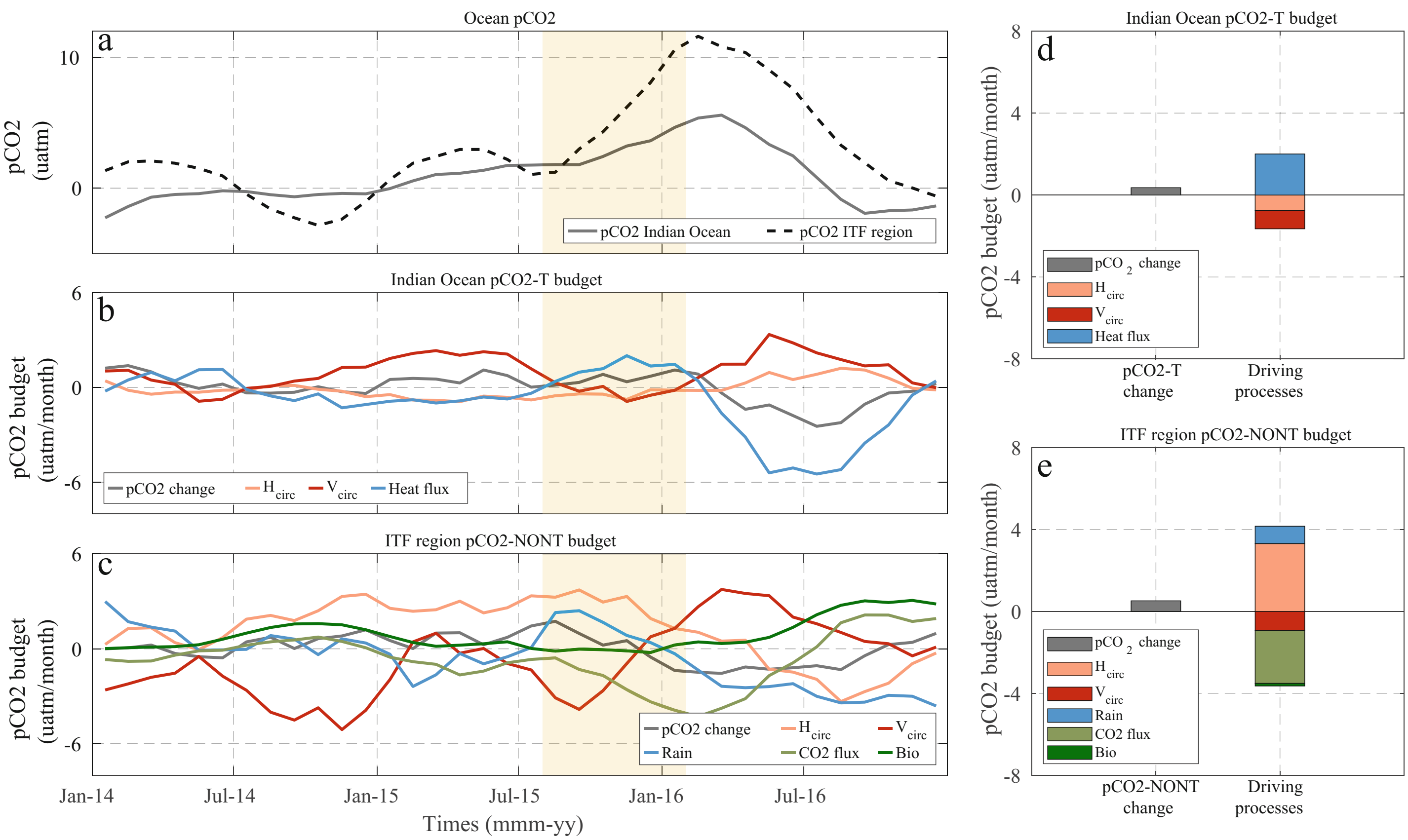

Fig. 4. Mechanisms controlling the pCO$_2$-T and pCO$_2$-NONT in the two subregions. (**a**) time series of ocean pCO$_2$ anomaly in the pCO$_2$-T and pCO$_2$-NONT regions. Time series of pCO$_2$-T (**b**) and pCO$_2$-NONT (**c**) budget averaged in the pCO$_2$-T and pCO$_2$-NONT regions respectively. Bar plot of pCO$_2$-T (**d**) and pCO$_2$-NONT (**e**) budget averaged in August 2015 and January 2016 in the two subregions. The subregion definition refers to Fig. 3. Yellow shading color in b and c highlights the period from August 2015 to January 2016 when ocean pCO$_2$ rapidly increases.

emerges as the dominant factor during the focus period (August 2015 to January 2016). Rainfall also exerts a significant influence in driving the positive ocean pCO$_2$ tendency, which aligns with the finding initially identified and quantified by Valsala et al. (2020). Other terms (H_{circ}, CO$_2$ flux, and Bio) partially offset the horizontal transport and rainfall terms (Supporting Information Fig. S14). Note that the chlorophyll interannual variability in this region (0.02 mg/m^3) is relatively minor compared with the Arabian Sea (−0.2 mg/m^3) and Bay of Bengal (−0.15 mg/m^3) between August 2015 and January 2016 (Supporting Information Fig. S15), which is consistent with Currie et al. (2013). This modest variability confirms the weak influence of biological process in the pCO$_2$-NONT region.

Budget analysis indicates the elevated ocean pCO$_2$ anomaly is primarily driven by horizontal transport in the southeastern Indian Ocean. As horizontal transport alone cannot induce a high ocean pCO$_2$ without external sources, a source of water with high ocean pCO$_2$ should be identified. Figure 3c, Supporting Information Fig. S12 illustrate a pronounced gradient of pCO$_2$-NONT, DIC, Alk, and SSS decreasing from the ITF strait (e.g., Lombok Strait, Sunda Strait, and Timor Sea) towards the Indian Ocean. This decreasing gradient suggests the ITF currents move high pCO$_2$, DIC, ALk, and SSS from the ITF strait to the southeastern Indian Ocean, aligning with pathways reported in earlier studies (Valsala and Maksyutov 2010; Valsala et al. 2010). This confirms the water source of high ocean pCO$_2$ originates from ITF region, which is probably related to the Pacific Ocean warm pool, driven by the extreme El Niño 2015. The high ocean pCO$_2$ anomaly in 2015 coincides well with the extreme ITF volume transport (Supporting Information Figs. S16, S17) which suggests an important role of ITF in the ocean carbon cycle in the southeastern Indian Ocean (Fritz et al. 2023). A further investigation reveals that the anomalous horizontal transport term is largely driven by ocean pCO$_2$ anomaly rather than the volume transport anomaly (Supporting Information Fig. S18).

Discussion and summary

A conventional IOD is characterized by a dipole anomaly, involving SST, wind, upwelling, and rainfall contrasts between the western and eastern Indian Ocean (Saji et al. 1999). The IOD in 2015 is distinct, with amplified warming in the west and central Indian Ocean (Supporting Information Fig. S12a), weakened cooling in the eastern Indian Ocean (Jiang et al. 2022), and unprecedented weakening ITF in the southeastern Indian Ocean. These unique processes are closely related to the co-occurrence of IOD and extraordinary El Niño in 2015 (Zhang et al. 2018; Jiang et al. 2022).

Owing to the unique dynamic processes, CO_2 flux in 2015 exhibits a unique response with an extremely weakened (positive) flux anomaly (Fig. 1). This CO_2 flux anomaly is governed by the increasing ocean $p$$CO_2$, which comprises two components: $p$$CO_2$-T and $p$$CO_2$-NONT (Fig. 2). Depending on their contributions to the positive ocean $p$$CO_2$, the Indian Ocean is separated into two subregions: $p$$CO_2$-T region dominated by $p$$CO_2$-T in the west and central Indian Ocean and the $p$$CO_2$-NONT region dominated by $p$$CO_2$-NONT in the southeastern Indian Ocean (Fig. 3). The amplified warming expands the $p$$CO_2$-T area, which significantly increases the positive ocean $p$$CO_2$ anomaly in the $p$$CO_2$-T region (Fig. 4). In the southeastern Indian Ocean, the $p$$CO_2$-NONT is driven by the ITF instead of upwelling under the influence of co-occurrence of IOD and extraordinary El Niño in 2015. The ocean $p$$CO_2$ gradient further confirms that the ITF currents move high $p$$CO_2$, DIC, ALk, and SSS from the ITF strait to the southeastern Indian Ocean (Fig. 4; Supporting Information Fig. S12). This is consistent with previous work that examined the effect of ITF on the distribution of salinity anomaly (Zhang et al. 2016; Kido and Tozuka 2017).

This study has identified a unique ocean carbon response to the extraordinary processes in 2015 IOD. Owing to the complex variability of IOD and its intricate interaction with El Niño, numerous uncertainties still exist in a complete understanding of air–sea CO_2 flux interannual variability in the Indian Ocean. The model captures a considerable extent of the ocean carbon interannual variability; yet, it exhibits biases stemming from the absence of interannual variability in river discharge and atmospheric deposition. There remains potential to further reduce these simulation biases through the ongoing advancements in terrestrial and atmospheric modeling, along with accumulation of observational data on river discharge and atmospheric deposition. As the positive IOD event keeps occurring (e.g., 2024) underlying climate warming, more direct observation data (cruises, BGC-Argo floats, and RAMA stations) are needed to accurately estimate CO_2 flux in the Arabian Sea, Somali coast, southeastern Indian Ocean, west and east equatorial Indian Ocean. Furthermore, conducting numerical experiments, such as scenarios with the ITF channel being either closed or open are necessary to quantify the role of ITF in the ocean carbon variability. Therefore, further studies are necessary for a comprehensive understanding of ocean carbon variability in the Indian Ocean between different combinations of IOD and El Niño.

References

Adcroft, A., and others. 2019. The GFDL Global Ocean and sea ice model OM4.0: Model description and simulation features. J. Adv. Model. Earth Syst. **11**: 3167–3211. doi:10.1029/2019MS001726

Aparna, S. G., J. P. McCreary, D. Shankar, and P. N. Vinayachandran. 2012. Signatures of Indian Ocean dipole and El Niño–southern oscillation events in sea level variations in the bay of Bengal. J. Geophys. Res. Oceans **117**: C10012. doi:10.1029/2012JC008055

Bakker, D. C. E., and others. 2016. A multi-decade record of high-quality fCO2 data in version 3 of the Surface Ocean CO2 atlas (SOCAT). Earth System Science Data **8**: 383–413. doi:10.5194/essd-8-383-2016

Chandra, N., and others. 2022. Estimated regional CO2 flux and uncertainty based on an ensemble of atmospheric CO2 inversions. Atmos. Chem. Phys. **22**: 9215–9243. doi:10.5194/acp-22-9215-2022

Currie, J. C., and others. 2013. Indian Ocean dipole and El Niño/southern oscillation impacts on regional chlorophyll anomalies in the Indian Ocean. Biogeosciences **10**: 6677–6698. doi:10.5194/bg-10-6677-2013

DeVries, T. 2022. Atmospheric CO2 and sea surface temperature variability cannot explain recent decadal variability of the ocean CO2 sink. Geophys. Res. Lett. **49**: e2021GL096018. doi:10.1029/2021GL096018

Doney, S. C., and others. 2009. Mechanisms governing interannual variability in upper-ocean inorganic carbon system and air–sea CO2 fluxes: Physical climate and atmospheric dust. Deep-Sea Res. II Top. Stud. Oceanogr. **56**: 640–655. doi:10.1016/j.dsr2.2008.12.006

Du, Y., W. Cai, and Y. Wu. 2013. A new type of the Indian Ocean dipole since the mid-1970s. J. Climate **26**: 959–972. doi:10.1175/JCLI-D-12-00047.1

Edwing, K., Z. Wu, W. Lu, X. Li, W.-J. Cai, and X.-H. Yan. 2024. Impact of marine heatwaves on Air-Sea CO2 flux along the US East Coast. Geophys. Res. Lett. **51**: e2023GL105363. doi:10.1029/2023GL105363

Friedlingstein, P., and others. 2022. Global carbon budget 2022. Earth Syst. Sci. Data **14**: 4811–4900. doi:10.5194/essd-14-4811-2022

Fritz, M., M. Mayer, L. Haimberger, and S. Winkelbauer. 2023. Assessment of Indonesian throughflow transports from ocean reanalyses with mooring-based observations. Ocean Sci. **19**: 1203–1223. doi:10.5194/os-19-1203-2023

Gregor, L., and N. Gruber. 2021. OceanSODA-ETHZ: A global gridded data set of the surface ocean carbonate system for seasonal to decadal studies of ocean acidification. Earth Syst. Sci. Data **13**: 777–808. doi:10.5194/essd-13-777-2021

Gruber, N., and others. 2023. Trends and variability in the ocean carbon sink. Nat. Rev. Earth Environ. **4**: 119–134. doi:10.1038/s43017-022-00381-x

Guo, F., Q. Liu, S. Sun, and J. Yang. 2015. Three types of Indian Ocean dipoles. J. Climate **28**: 3073–3092. doi:10.1175/JCLI-D-14-00507.1

Guo, F., Q. Liu, J. Yang, and L. Fan. 2018. Three types of Indian Ocean Basin modes. Climate Dynam. **51**: 4357–4370. doi:10.1007/s00382-017-3676-z

Huang, L., W. Zhuang, W. Lu, Y. Zhang, D. Edwing, and X.-H. Yan. 2024. Rapid Sea level rise in the tropical Southwest Indian Ocean in the recent two decades. Geophys. Res. Lett. **51**: e2023GL106011. doi:10.1029/2023GL106011

Jabaud-Jan, A., N. Metzl, C. Brunet, A. Poisson, and B. Schauer. 2004. Interannual variability of the carbon dioxide system in the southern Indian Ocean (20° S–60° S): The impact of a warm anomaly in austral summer 1998. Global Biogeochem. Cycles **18**: GB1042. doi:10.1029/2002GB002017

Jiang, J., Y. Liu, J. Mao, J. Li, S. Zhao, and Y. Yu. 2022. Three types of positive Indian Ocean dipoles and their relationships with the south Asian summer monsoon. J. Climate **35**: 405–424. doi:10.1175/JCLI-D-21-0089.1

Kartadikaria, A. R., and others. 2015. CO2 sink/source characteristics in the tropical Indonesian seas. J. Geophys. Res. Oceans **120**: 7842–7856. doi:10.1002/2015JC010925

Kido, S., and T. Tozuka. 2017. Salinity variability associated with the positive Indian Ocean dipole and its impact on the Upper Ocean temperature. J. Climate **30**: 7885–7907. doi:10.1175/JCLI-D-17-0133.1

Landschützer, P., N. Gruber, D. C. E. Bakker, and U. Schuster. 2014. Recent variability of the global ocean carbon sink. Global Biogeochem. Cycles **28**: 927–949. doi:10.1002/2014GB004853

Le Quéré, C., J. C. Orr, P. Monfray, O. Aumont, and G. Madec. 2000. Interannual variability of the oceanic sink of CO2 from 1979 through 1997. Global Biogeochem. Cycles **14**: 1247–1265. doi:10.1029/1999GB900049

Liao, E., L. Resplandy, J. Liu, and K. W. Bowman. 2020. Amplification of the ocean carbon sink during El Niños: Role of poleward Ekman transport and influence on atmospheric CO2. Global Biogeochem. Cycles **34**: e2020GB006574. doi:10.1029/2020GB006574

Mayer, M., M. Alonso Balmaseda, and L. Haimberger. 2018. Unprecedented 2015/2016 Indo-Pacific heat transfer speeds up tropical Pacific heat recharge. Geophys. Res. Lett. **45**: 3274–3284. doi:10.1002/2018GL077106

McKinley, G. A., A. R. Fay, Y. A. Eddebbar, L. Gloege, and N. S. Lovenduski. 2020. External forcing explains recent decadal variability of the ocean carbon sink. AGU Adv. **1**: e2019AV000149. doi:10.1029/2019AV000149

Metzl, N., F. Louanchi, and A. Poisson. 1998. Seasonal and interannual variations of sea surface carbon dioxide in the subtropical Indian Ocean. Mar. Chem. **60**: 131–146. doi:10.1016/S0304-4203(98)00083-8

Rixen, T., V. Ittekkot, B. Herunadi, P. Wetzel, E. Maier-Reimer, and B. Gaye-Haake. 2006. ENSO-driven carbon see saw in the Indo-Pacific. Geophys. Res. Lett. **33**: L07606. doi:10.1029/2005GL024965

Sabine, C. L., and others. 2004. The oceanic sink for anthropogenic CO2. Science **305**: 367–371. doi:10.1126/science.1097403

Saji, N. H., B. N. Goswami, P. N. Vinayachandran, and T. Yamagata. 1999. A dipole mode in the tropical Indian Ocean. Nature **401**: 360–363. doi:10.1038/43854

Sarma, V. V. S. S. 2006. The influence of Indian Ocean dipole (IOD) on biogeochemistry of carbon in the Arabian Sea during 1997–1998. J. Earth Syst. Sci. **115**: 433–450. doi:10.1007/BF02702872

Sarma, V. V. S. S., Y. S. Paul, D. G. Vani, and V. S. N. Murty. 2015. Impact of river discharge on the coastal water pH and pCO2 levels during the Indian Ocean dipole (IOD) years in the western bay of Bengal. Cont. Shelf Res. **107**: 132–140. doi:10.1016/j.csr.2015.07.015

Sarma, V. V. S. S., and others. 2023. Air-Sea fluxes of CO2 in the Indian Ocean between 1985 and 2018: A synthesis based on observation-based surface CO2, hindcast and atmospheric inversion models. Global Biogeochem. Cycles **37**: e2023GB007694. doi:10.1029/2023GB007694

Shanthi, R., D. Poornima, T. Thangaradjou, A. Saravanakumar, S. B. Choudhury, and R. Roy. 2022. Decadal variability of satellite-derived Air–Sea CO2 flux in southwestern part of the bay of Bengal. Ocean Sci. J. **57**: 211–223. doi:10.1007/s12601-022-00063-1

Stock, C. A., and others. 2020. Ocean biogeochemistry in GFDL's earth system model 4.1 and its response to increasing atmospheric CO2. J. Adv. Model. Earth Syst. **12**: e2019MS002043. doi:10.1029/2019MS002043

Takahashi, T., J. Olafsson, J. G. Goddard, D. W. Chipman, and S. C. Sutherland. 1993. Seasonal variation of CO2 and nutrients in the high-latitude surface oceans: A comparative study. Global Biogeochem. Cycles **7**: 843–878. doi:10.1029/93GB02263

Valsala, V., and S. Maksyutov. 2010. A short surface pathway of the subsurface Indonesian throughflow water from the Java coast associated with upwelling, Ekman transport, and subduction. Int. J. Oceanogr. **2010**: 540783. doi:10.1155/2010/540783

Valsala, V., S. Maksyutov, and R. Murtugudde. 2010. Possible interannual to interdecadal variabilities of the Indonesian throughflow water pathways in the Indian Ocean. J. Geophys. Res. Oceans **115**: C10016. doi:10.1029/2009JC005735

Valsala, V., and S. Maksyutov. 2013. Interannual variability of the air–sea CO2 flux in the north Indian Ocean. Ocean Dyn. **63**: 165–178. doi:10.1007/s10236-012-0588-7

Valsala, V., M. G. Sreeush, and K. Chakraborty. 2020. The IOD impacts on the Indian Ocean carbon cycle. J. Geophys. Res. Oceans **125**: e2020JC016485. doi:10.1029/2020JC016485

Valsala, V., and others. 2021. An observing system simulation experiment for Indian Ocean surface pCO2 measurements. Prog. Oceanogr. **194**: 102570. doi:10.1016/j.pocean.2021.102570

Xiao, F., D. Wang, and M. Y. T. Leung. 2020. Early and extreme warming in the South China Sea during 2015/2016: Role of an unusual Indian Ocean dipole event. Geophys. Res. Lett. **47**: e2020GL089936. doi:10.1029/2020GL089936

Yang, G. G., and others. 2024. Can three-dimensional nitrate structure be reconstructed from surface information with artificial intelligence? A proof-of-concept study. Sci. Total Environ. **924**: 171365. doi:10.1016/j.scitotenv.2024.171365

Zhang, L., Y. Du, and W. Cai. 2018. Low-frequency variability and the unusual Indian Ocean dipole events in 2015 and 2016. Geophys. Res. Lett. **45**: 1040–1048. doi:10.1002/2017GL076003

Zhang, L., W. Han, Y. Li, and N. S. Lovenduski. 2019. Variability of sea level and Upper-Ocean heat content in the Indian Ocean: Effects of subtropical Indian Ocean dipole and ENSO. J. Climate **32**: 7227–7245. doi:10.1175/JCLI-D-19-0167.1

Zhang, Y., Y. Du, and T. Qu. 2016. A sea surface salinity dipole mode in the tropical Indian Ocean. Climate Dynam. **47**: 2573–2585. doi:10.1007/s00382-016-2984-z

Acknowledgments

This work is supported by the project of Southern Marine Science and Engineering Guangdong Laboratory (Zhuhai) (Grant number: SML2023SP219), Shanghai Pujiang Program (Grant number: 22PJ1406300), the Global Change and air–sea Interaction Project (Grant number: GASI-04-QYQH-02), the National Natural Science Foundation of China (Grant numbers: 42176051; 42376048), the Taishan Scholars Program (Grant number: tsqn202306294), the Ocean Negative Carbon Emissions (ONCE) Program, and Shanghai Frontiers Science Center of Polar Science (E.L.). We acknowledge the National Centers for Environmental Information for providing the World Ocean Atlas data. E.L thanks the Center for High Performance Computing at Shanghai Jiao Tong University for the support of model computations and results analysis on the Siyuan-1 cluster. We acknowledge the Surface Ocean CO_2 Atlas data (SOCAT; www.socat.info), which is a uniformly quality-controlled surface ocean CO_2 database. The SOCAT data is an international effort, endorsed by the International Ocean Carbon Coordination Project (IOCCP), the Surface Ocean Lower Atmosphere Study (SOLAS), and the Integrated Marine Biogeochemistry and Ecosystem Research program (IMBER).

Submitted 23 September 2023
Revised 29 March 2024
Accepted 02 April 2024